Hydrophobic–Hydrophilic Surfaces Exhibiting Dropwise Condensation for Anti-Soiling Applications

Illya Nayshevsky, *Student Member, IEEE*, QianFeng Xu, and Alan M. Lyons

***Abstract*—Soiling of solar cover glass is a significant challenge that increases the levelized cost of electricity of solar photovoltaic energy through loss of electrical output and/or increased operation and maintenance costs. Hydrophobic coatings can reduce the cost of cleaning, but an external source of cleaning water is still required. Dew, however, can be harnessed to create a self-cleaning glass surface. To efficiently use condensation (i.e., natural dew) to create a self-cleaning glass surface, we fabricated a hybrid hydrophobic–hydrophilic coating, with an array of isolated hydrophilic circular rings. Water roll-off collection rates were measured in a simulated dew environment. The effect of hydrophilic ring geometry (location, arrangement, diameter, distance, and count) was studied to determine the optimal cleaning efficiency. The hybrid surface increased water collection rates by 95% over an uncoated (bare) glass surface and 51% compared with uniformly coated hydrophobic low-iron glass.**

***Index Terms*—Coatings, photovoltaic panels, solar cover glass.**

I. Introduction

SOILING of solar cover glass is reported as one of the major sources of photovoltaic efficiency loss [1]. The annual soiling loss averaged over one year is assumed to be 5% in National Renewable Energy Laboratory's current and long-term levelized cost of electricity input assumptions for the SunShot 2030 targets of 3–5 ¢/kWh [2]. In regions with heavy soiling, the annual soiling loss can be as high as 50% [3].

Manuscript received June 7, 2018; revised October 12, 2018; accepted November 16, 2018. Date of publication December 5, 2018; date of current version December 21, 2018. This work was supported as part of Durable Module Materials Consortium funded by the United States Department of Energy, Office of Energy Efficiency and Renewable Energy, Solar Energy Technologies Office, under Grant 32509. The work of I. Nayshevsky was supported in part by the Graduate Center of the City University of New York and the College of Staten Island, City University of New York. *(Corresponding author: Alan M. Lyons.)*

I. Nayshevsky is with the College of Staten Island, City University of New York, Staten Island, NY 10314 USA, and also with the Graduate Center of the City University of New York, New York, NY 10016 USA (e-mail: illya.nayshevsky@csi.cuny.edu).

Q. Xu is with the College of Staten Island, City University of New York, Staten Island, NY 10314 USA, and also with ARL Designs LLC, New York, NY 10027 USA (e-mail: qianfengxu@gmail.com).

A. M. Lyons is with the College of Staten Island, City University of New York, Staten Island, NY 10314 USA, with the Graduate Center of the City University of New York, New York, NY 10016 USA, and also with ARL Designs LLC, New York, NY 10027 USA (e-mail: alan.lyons@csi.cuny.edu).

Color versions of one or more of the figures in this paper are available online at http://ieeexplore.ieee.org.

Digital Object Identifier 10.1109/JPHOTOV.2018.2882636

In light rain and morning dew conditions, water evaporates before it can roll off the surface; this process accelerates the formation of chemical and physical bonds between dust and glass [4]. These reactions increase the magnitude and duration of efficiency losses and require mechanical force or the use of detergents to remove the soil from the surface of the glass [1]. Dew has been associated with accelerated dust accumulation in both Arizona [5], [6], as well as the Europe, the Middle East and Africa (EMEA) region [1], [7], [8]. Work has been reported to reduce soiling losses by modifying glass surfaces with either hydrophobic or hydrophilic coatings [4], [7].

Our group has shown that a hydrophobic coating on glass (water contact angle (WCA) of $\geq 90°$ and a contact angle hysteresis (CAH) $<40°$) reduces soiling rates compared with bare glass surfaces in artificial dew conditions [9]. Optical losses due to dust deposition were reduced by 45% compared with dust-coated bare glass. A dust herding mechanism was identified to account for this anti-soiling property. On bare glass, filmwise condensation was observed, where water condenses to form a continuous layer of water, uniformly covering the glass surface. Upon evaporation, dust is spread and redeposited over the entire surface. In contrast, on the hydrophobic coated surface, water condenses in a dropwise manner. As the droplets grow, they imbibe dust on the surface. During evaporation, the droplets shrink laterally, which concentrates the dust into the centers of each former water drop, resulting in improved light transmission performance.

To completely clean hydrophobic coated glass in natural dew conditions, these dust-containing droplets need to grow to a critical size so that they can slide off the surface before drying out. Recently, we have demonstrated that a hybrid superhydrophobic–hydrophilic surface can accelerate the growth and roll-off of water droplets on hydrophilic needles [10]. The water collection rate was quadrupled compared with a uniform hydrophilic surface and doubled compared with hydrophobic or superhydrophobic surfaces.

In this study, we describe the fabrication of hydrophilic patterns on hydrophobic coated solar cover glass, with a purpose of increasing dew collection efficiency and ultimately reducing soiling rates. The effect of hydrophilic ring geometry, including array conformation, number of rows of features, and feature diameter, on water condensation rates under artificial dew conditions is presented.

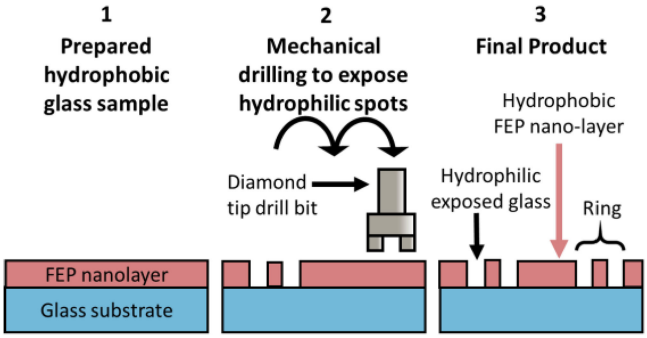

Fig. 1. Schematic of hybrid hydrophobic–hydrophilic surface preparation. The process utilizes mechanical drilling to produce hydrophilic features of defined parameters on a hydrophobic surface.

II. Methods

A. Sample Fabrication

Low-iron soda-lime glass, 3 mm thick, was cut to size (58 mm $\times$ 58 mm), washed, and dried. A thin hydrophobic fluoropolymer coating was applied onto glass using a chemical vapor deposition technique. Briefly, a clean glass sample was placed orthogonal to, and 5 cm above, a piece of fluorinated ethylene propylene (FEP) measuring 5 cm $\times$ 5 cm $\times$ 0.5 cm. The chamber was sealed and heated at 320 °C (60 °C above the melt temperature) for 1 h. Thermal decomposition species from FEP deposited and bonded to the glass, resulting in a robust hydrophobic surface that can withstand condensation conditions. The WCA of the surface after coating on the tin side is $97° \pm 6°$ with a CAH value of $46° \pm 12°$. Hydrophilic rings were formed using a mechanical drill secured to a Jenome JR2200N robot. Hollow cylindrical diamond drill-bits, 1, 2, and 3.2 mm in diameter, were used to cut through the coating and 200 μm into the glass to create hydrophilic rings in a programmed array (see Figs. 1 and 2). Program variables evaluated include geometric (packing) arrangement [see Fig. 2(a)], the number of rows of hydrophilic features [see Fig. 2(b)], the edge-to-edge distance between hydrophilic features [see Fig. 2(c)], and the diameter of hydrophilic features [see Fig. 2(d)]. After drilling, the samples were rinsed with deionized water to remove contaminants resulting from the drilling process. The size of hydrophilic features was determined from optical images.

B. Condensation Chamber

The condensation experiments were conducted in a Delrin/Acrylic chamber, specifically built for these experiments (see Fig. 3). Hybrid-coated glass samples were mounted onto an aluminum plate measuring 5.0 cm $\times$ 5.0 cm $\times$ 0.75 cm thick. A digital thermometer integrated circuit within a 6.0-mm outside diameter (o.d.) stainless steel sheath (digital thermometer IC) (Maxim Integrated DS18B20) was mounted inside the aluminum heat-spreader. This heat spreader was mounted onto a 60-W Peltier thermoelectric cooler (TEC) (Laqiya TEC1-12706). An aluminum heatsink along with a CPU fan was mounted under the TEC to remove heat from the hot side of the TEC. The heatsink/fan, TEC, and aluminum heat spreader

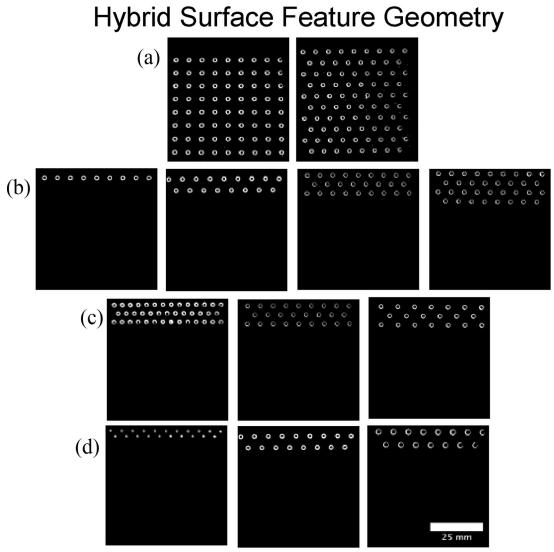

Fig. 2. Top-down photographs (computer enhanced) of coated glass surfaces showing: (a) geometric arrangement (square vs. staggered), 2-mm o.d., 4-mm distance between features; (b) number of rows (1, 2, 3, 4, and 10), 2-mm o.d., 4-mm distance between features; (c) distances between hydrophilic rings (2, 4, 6 mm), 2-mm o.d., three rows; and (d) diameters of hydrophilic rings (1.0, 2.0, 3.2 mm), 4-mm distance between features, two rows.

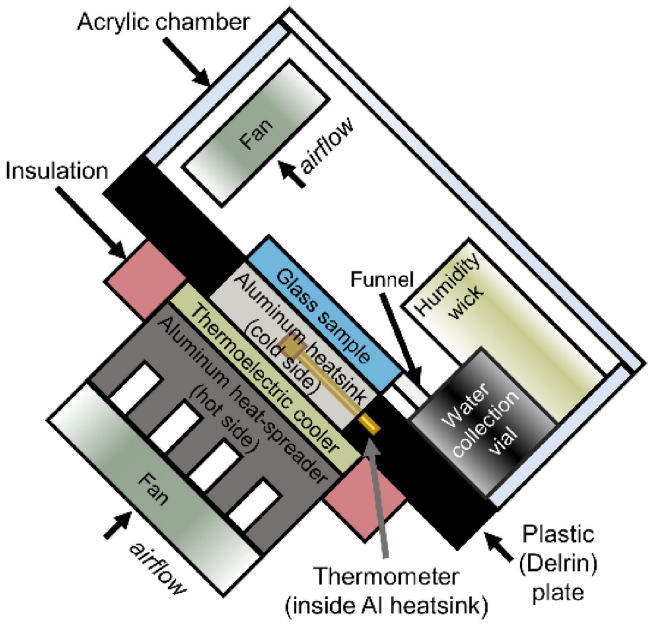

Fig. 3. Cross-sectional schematic of the condensation chamber including the TEC system, the water collection scheme, and the humidification system (not to scale).

were secured to the Delrin back-plate with springs. Thermal grease was used in all interfaces to enhance thermal conductivity (Wakefield Solutions, Inc., Type 126 Non-Silicone Thermal Joint Compound). The temperature of the TEC was controlled via a digital thermometer IC located in the heat spreader and a 10-A 12-VDC relay (Songle SRD-05VDC-SL-C) connected to a Raspberry Pi 3 microcontroller, using a python script.

The entire substrate–TEC assembly was mounted into the base of the environmental chamber, which was constructed from

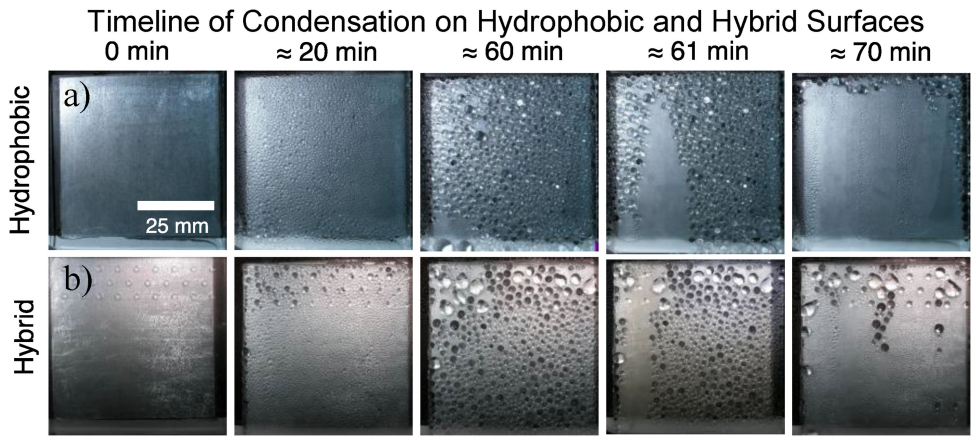

Fig. 4. Timeline of condensation on (a) hydrophobic (control) and (b) hybrid hydrophobic–hydrophilic surface. The hybrid surface contains three rows of 2-mm-diameter hydrophilic features, which are spaced at 4-mm distance (edge-to-edge). Visual analysis shows increased condensation and greater water drop diameters on hydrophilic rings when compared with the hydrophobic (control) sample.

a 25.4 cm × 25.4 cm × 0.25 cm Delrin plate, with a machined opening of 5.0 cm × 5.0 cm in the center. The Delrin plate was mounted at a 45° angle. An acrylic enclosure (LWH: 18 cm × 18 cm × 10 cm) with a silicone gasket was used to isolate the system. The atmosphere inside the enclosure was saturated with water vapor using a wick cut from a Honeywell HC22P Humidifier Pad, which was partially immersed in a beaker of deionized water. A low-velocity fan (Thermaltake Mobile Fan II) was mounted to the top of the chamber.

The relative humidity was measured with a dry bulb/wet bulb method using two digital thermometer ICs, housed in 6-mm-diameter stainless steel sheaths, which were connected to the microcontroller. Water condensate was collected with a home-made superhydrophobic water collection channel and a 50-mL 3-D printed plastic beaker, tared before use.

C. Experimental Methods

WCA measurements were obtained using a ráme-hart 250-F1 goniometer with a 5-μL drop of water. Images of the surface were recorded with a Nikon Coolpix P2 camera at 1-min time increments; the resolution of images was 2048 × 1536 pixels. Condensation experiments were conducted by first placing the glass sample onto the aluminum heat spreader. A thin film of water between glass and aluminum was used as the interface material, since this eliminates the potential for surface contamination. The acrylic lid to the chamber was secured, and the temperature of the aluminum heat spreader was reduced to 10 °C. The TEC cooled the heat spreader to 10 °C within 10 min. The temperature of the air inside the chamber was maintained at 23.0 °C (±0.9 °C) without additional controls. The relative humidity inside the chamber increased to 89.9% (±1.4%) within 6 min after the chamber was closed. Condensation on the samples was monitored for 10–20 h. Water that condensed and slid-off the surface via gravity was collected and the mass measured at the end of the experiment.

Images of the condensation process were analyzed to determine the diameter and location of the water drop that initiated the water slide-off event. The analysis was conducted via a computer vision algorithm written in python 3 and utilizing Open Source Computer Vision Library for image processing.

III. Results

A. Bare Glass vs. Hydrophobic Glass

As expected, filmwise condensation was observed on the hydrophilic bare glass samples, while dropwise condensation was observed on the hydrophobic samples. On bare glass, micrometer-size droplets that formed initially merged into a continuous film within the first 20 min. This continuous liquid film was maintained for the duration of the experiment. Bare clean glass exhibits a water collection rate of 4.7 ± 1.8 × 10^{-3} mg/mm^2·min, which corresponds to 11.2 mL of water over a typical 12.2-h experiment.

In contrast, the hydrophobic coated glass sample exhibits a condensation rate of 6.7 ± 0.6 × 10^{-3} mg/mm^2·min, which is an increase of 42% over bare glass. Droplets nucleate and grow on the hydrophobic surface, as shown in Fig. 4(a). After 20 min, the droplets grow to an average diameter of ∼1.5 mm. Over time, the droplets continue to grow and merge through an Ostwald ripening process, resulting in a smaller number of droplets with larger diameters (2.2 ± 0.6 mm). As drop coalescence proceeds, larger droplets grow until they reach a critical size (3.9 ± 0.2 mm). At that point, the gravitational forces are sufficient to overcome the wetting forces along the solid–liquid–vapor triple contact line (TCL) and the droplet slides off the surface, imbibing droplets along its downward linear path, as shown in the fourth panel of Fig. 4(a). This leaves a swath of surface free of droplets, allowing the nucleation and growth process to restart. The last panel of Fig. 4(a) shows a surface that has been swept clear of most of the original droplets after 70 min, with new droplets at various stages of growth.

B. Water Collection Rates on Hybrid Hydrophobic–Hydrophilic Surfaces

Condensation on a hybrid surface proceeds by a combination of the hydrophilic and hydrophobic mechanisms described in

TABLE I
EFFECT OF SURFACE CHEMISTRY AND STRUCTURE ON CONDENSATION WATER COLLECTION

Sample [Type (feature diameter-distance between features-count of rows)]	Number of Trials [n]	Water Contact Angle [°]	Number of Hydrophilic Rings [n]	Number of rows [n]	Hydrophilic Ring Diameter [mm]	Distance Between Hydrophilic Rings [mm]	Critical Drop Diameter [mm]	Water Collection Rate [mg/mm^2 min] $\cdot 10^{-3}$
Hydrophobic (Control)	6	96±5	-	-	-	-	3.9±0.2	6.7±0.6
Bare Glass (Control)	7	<10	-	-	-	-	-	4.7±1.8
Hybrid (2mm-4mm-1row)	3	95±4	9	1	1.9±0.2	4.0±0.5	-	6.6±1.3
Hybrid (2mm-4mm-2rows)	5	98±3	17	2			4.6±1.2	8.6±0.7
Hybrid (2mm-4mm-3rows)	6	97±5	26	3			-	9.1±0.6
Hybrid (2mm-4mm-4rows)	3	97±3	34	4			-	8.7±0.3
Hybrid (2mm-4mm-10rows)	3	96±4	85	10			-	7.8±0.2
Hybrid (1mm-4mm-2rows)	3	97±3	21	2	1.1±0.1		4.4±0.8	7.2±1.1
Hybrid (3mm-4mm-2rows)	3	97±2	15		3.2±0.1		5.1±0.5	8.0±0.5
Hybrid (2mm-2mm-3rows)	3	95±5	41	3	1.9±0.2	2.0±0.4	-	9.2±1.4
Hybrid (2mm-6mm-3rows)	3	98±4	20			6.0±0.5	-	8.7±0.2
Hybrid (2mm-4mm-8rows) -square	3	97±5	64	8		4.0±0.5	-	7.9±0.8

the previous section. Nucleation of water droplets occurs on both regions, but as shown in the second panel of Fig. 4(b), the liquid droplets initially grow more rapidly on the hydrophilic rings. As the experiment progresses, larger droplets form in these locations, as seen in the third panel of Fig. 4(b). The shape of these droplets is a distorted teardrop because of the strong pinning forces along the hydrophilic TCL that counter the gravitational attraction of the mass of water. Some large droplets have merged and become pinned to two hydrophilic rings, further increasing the TCL that must be overcome before sliding. After 70 min, most of the large droplets have rolled-off the surface, and a new cycle of nucleation and growth has progressed, as seen in the last panel of Fig. 4(b).

In the following sections, the effect of hydrophilic ring array geometry, number of rows of features, pitch of features, and diameter of rings is discussed in detail.

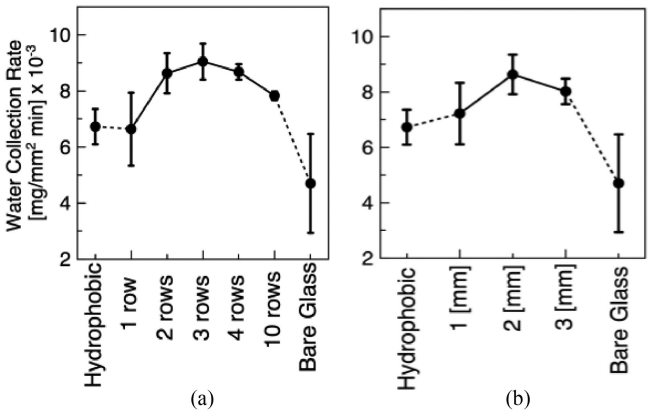

Fig. 5. Water collection rates as function of (a) the number of rows of 2.0-mm-diameter hydrophilic ring features and (b) the diameter of two rows of hydrophilic features. All features spaced 4.0 mm apart.

C. Water Collection: Staggered vs. Square Arrays of Hydrophilic Rings

Staggered arrays of the drilled hydrophilic rings were compared with square arrays using samples with rows of features covering the full surface of the glass substrate, as shown in Fig. 2(a). The ring o.d. is 2 mm, with 4 mm of space between adjacent ring perimeters. As shown in Table I, the water collection rates are $7.9 \pm 0.8 \times 10^{-3}$, $7.8 \pm 0.2 \times 10^{-3}$, and $6.7 \pm 0.6 \times 10^{-3}$ mg/mm$^2\cdot$min for staggered arrays, square arrays, and the hydrophobic control, respectively. The water collection rates of hybrid surfaces with staggered and square arrays are similar to each other, but $\sim$17% higher than the hydrophobic control. This result demonstrates that hydrophilic ring arrays can increase the water collection rates, and the difference between different array conformations is not significant. A staggered arrangement of hydrophilic features was used to evaluate the effect of other parameters in all further experiments in this paper (see Table I).

D. Water Collection: Number of Rows of Hydrophilic Features

Although coverage of the full surface could increase the number of slide-off events, a larger number of hydrophilic features could also be disadvantageous because a larger number of growing droplets would locally decrease water concentration in the vapor near the glass surface under nature/artificial dew conditions. Observations of condensation on hydrophobic surfaces [see Fig. 4(a)] showed that drops rolling-off from the uphill portion of the surface carry away droplets along its down-slope path, decreasing the impact of down-slope rows. Thus, the effect of the number of rows of hydrophilic rings was systematically evaluated by staring from the top of the glass sample.

Water collection rate as a function of number of rows of hydrophilic features is shown in Fig. 5(a). For this evaluation, all hydrophilic rings have a diameter of 2 mm with an edge-to-edge separation distance of 4 mm. Average and standard deviation values from at least three trials is plotted.

A maximum water collection rate was observed for the sample with three rows of hydrophilic regions ($9.1 \pm 0.6 \times 10^{-3}$ mg/mm$^2\cdot$min) [see Fig. 4(a)]. This value is 36% greater than a hydrophobic surface without hydrophilic rings and more than twice the value on hydrophilic (bare) glass. Increasing the number of rows further resulted in a gradual decrease in water collection rates.

E. Water Collection: Distance Between Features

The effect of edge-to-edge spacing on water collection rates was measured for spacing values of 2, 4, and 6 mm with the hydrophilic ring diameter fixed at 2 mm. Almost the same high water collection rate was maintained for hybrid surfaces with 2- and 4-mm feature spacing between hydrophilic rings, and a small decrease ($\sim$5%) was observed when the spacing feature was increased to 6 mm (see Table I). This may be due to a tradeoff between local water vapor concentration and number of hydrophilic nucleation sites.

F. Water Collection: Feature Diameter

The dependence of water collection rates on the diameter of the hydrophilic rings is shown in Fig. 5(b). The distance between features was held at 4 mm, with two rows of features for all samples. A maximum rate was observed for 2-mm-diameter hydrophilic rings ($8.6 \pm 0.7 \times 10^{-3}$ mg/mm$^2 \cdot$min); both smaller (1 mm) and larger (3 mm) ring diameters reduced water collection rates by 19% and 8%, respectively.

The decreased rate for the 3-mm-diameter feature could be due to the longer TCL, requiring a larger droplet mass before roll-off. However, the water collection rate for the surface with the 1-mm-diameter feature dropped even more and was very close to hydrophobic surface without hydrophilic regions. This result indicates that the hydrophilic features must be above a certain size to accelerate the water collection rate. Further experiments to explore the effect of hydrophilic shape and size are underway.

G. Roll-Off Location and Critical Droplet Diameter

Visual and qualitative observations have shown that hydrophilic features serve as efficient droplet nucleation and growth locations on the hybrid samples (see Fig. 4) and increase water collection rates (see Table I). To quantify the impact of hydrophilic rings on the condensation process and the water collection rate, data from the camera images were analyzed to determine both the diameter and location of droplets that initiated roll-off events.

Fig. 6(a) shows the results for the hydrophobic control surface. The median critical droplet roll-off diameter was found to be 3.9 $\pm$ 0.2 mm. This value was independent of slide-off location; droplets that rolled-off from the top of the glass sample were within 0.1 mm of those that rolled-off from the bottom of the sample. Droplet diameters remained constant over the duration of the experiment. Fig. 6(a) also shows that droplets roll-off primarily from the top third of the substrate.

In contrast, the hydrophilic rings of the hybrid surface affect both the diameter and the location of the critical droplet volume. As shown in Fig. 6(b) and Table II, the droplets that form on the hydrophilic rings are 4.6 mm in diameter. This value represents an 18% increase, corresponding to 64% greater mass, than droplets formed on the control hydrophobic surface. The size of the droplets remains constant throughout the 15-mm region that contains hydrophilic rings. Below this location, the critical droplet diameter decreases abruptly to 3.4 mm, which is 13% smaller than the critical drop size on the control surface.

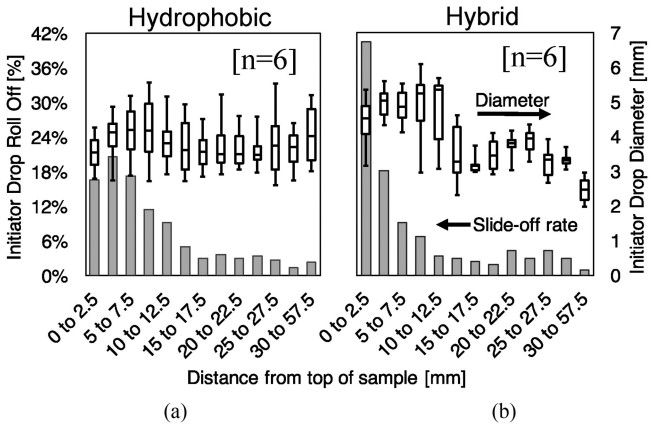

Fig. 6. Computational analysis of water drop diameter (right-hand axis) and location of the drop initiating the roll-off event (left-hand axis) for (a) hydrophobic control and (b) hybrid surface with three rows of 2-mm-diameter rings spaced 4 mm apart.

TABLE II
WATER DROP DIAMETER AT ROLL-OFF

Location	Hydrophobic [mm]	Hybrid [mm]
Entire sample	3.9±0.2	4.4±1.1
Top of sample (<15mm)	3.9±0.2	4.6±1.2
Bottom of sample (>15mm)	3.8±0.2	3.4±0.3

Not only do the hydrophilic rings increase drop diameter, but they also cause the critical droplet roll-off events to initiate from the top of the sample. Forty percent of roll-off events are observed within the top 2.5 mm of the surface, whereas only 17% of drops roll off from this location on the control hydrophobic surface.

IV. DISCUSSION

To increase condensation rates, hydrophilic regions were intentionally created on hydrophobic coated surfaces. Hydrophilic regions enhance condensation rates for several reasons. Nucleation of liquid water occurs more rapidly on a hydrophilic surface compared with a hydrophobic one. The enhancement ratio is significant and can exceed 10^{49} [10], [11]. Once a liquid water droplet nucleates, it will grow rapidly because the condensation rate on a hydrophilic surface, such as liquid water, is much greater than on a hydrophobic surface. Most importantly, larger liquid water droplets will grow at a faster rate than smaller diameter droplets because the vapor pressure of a droplet is an inverse function of droplet radius. Smaller droplets have a higher vapor pressure than larger droplets [12]. Thus, larger water drops grow at the expense of the smaller ones. This mechanism leads to Ostwald ripening, as shown in Fig. 4.

For a droplet to roll off the substrate, gravitational attraction must overcome the forces at the TCL that pin the droplet to the surface. These TCL forces are greater on hydrophilic surfaces and scale with increasing TCL length. Thus, larger hydrophilic features require more massive droplets before roll-off can occur.

The optimal number and size of the hydrophilic features are thus a tradeoff between condensation rates and TCL forces. Larger hydrophilic regions will nucleate liquid water rapidly, exhibit the lowest vapor pressures and fastest growth rates, and generate larger diameter droplets that would clean a larger swath of surface. However, the TCL line will be longer for these larger diameters, requiring a greater mass before roll-off could occur. The experimental results presented in this paper show that a hydrophilic ring diameter of 2 mm is optimal, maximizing water collection rates.

A larger number of growing droplets could reduce the concentration of water molecules in the vapor phase near the surface of the glass. This diffusion limit could, in turn, reduce overall condensation rates, favoring fewer rather than a larger number/density of nucleation sites. Our experimental results indicate that three rows of 2-mm-diameter features are optimal, which further contributes to higher water collection rates. Other geometrical variables, such as spacing between features and packing geometry, were not observed to significantly affect water collection rates.

Two other factors could also influence water collection rates: CAH of the hydrophobic coating and tilt angle of the glass. The chemistry and morphology of the hydrophobic coating can be tuned to reduce the CAH and thus the critical angle for droplets to slide-off the surface, as described by the Furmidge equation modified by Extrand and Gent [14]. For any given coating, increasing tilt angle will decrease the critical drop diameter [10]. We have recently developed a new method for forming fluoropolymer coatings on glass [15] that exhibit a CAH of $<15°$. Lower CAH coatings would reduce the tilt angle of the glass required for droplets to slide-off the surface as well as decrease the critical droplet size. Such new materials thus hold the promise of extending the range of geographical locations, where hybrid coatings can exploit dew to achieve self-cleaning properties to most latitudes. The properties of such new coatings are currently under investigation.

V. Conclusion

Creating surfaces with arrays of hydrophilic features on a hydrophobic coating demonstrate higher water collection rates compared with uncoated (bare) glass or uniformly hydrophobic coatings. Preferential nucleation of liquid water on hydrophilic regions and the high mobility of droplets on hydrophobic regions combine to increase water collection rates by a factor of 2 compared with uncoated glass. The hydrophilic rings were shown to increase not only the overall water collection efficiency, but also led to an increased diameter of the droplets rolling off the surface and caused these roll-off events to preferentially occur along the top surface of the sample. These effects are expected to increase the efficacy of self-cleaning from dew.

Although drilling proved useful for this study, it is obviously not the preferred method for creating hydrophilic patterns on glass due to the cost, scattering of light, and potential for initiating cracks. More feasible methods for creating hydrophilic patterns have recently been developed in our laboratory; these methods will be used in our subsequent work, in which anti-soiling properties of hybrid surfaces will be quantified. Future work will also evaluate scaling these effects on larger glass panels.

Acknowledgment

The views expressed in the article do not necessarily represent the views of the United States Department of Energy or the United States Government. The United States Government retains and the publisher, by accepting the article for publication, acknowledges that the United States Government retains a nonexclusive, paid-up, irrevocable, worldwide license to publish or reproduce the published form of this work, or allow others to do so, for United States Government purposes.

References

[1] T. Sarver, A. Al-Qaraghuli, and L. L. Kazmerski, "A comprehensive review of the impact of dust on the use of solar energy: History, investigations, results, literature, and mitigation approaches," *Renew. Sustain. Energy Rev.*, vol. 22, pp. 698–733, 2013.

[2] M. Woodhouse *et al.*, "On the path to sunshot: The role of advancements in solar photovoltaic efficiency, reliability, and costs," Nat. Renew. Energy Lab. Golden, CO, USA, Tech. Rep. NREL/TP-6A20-65872.

[3] H. Qasem, "Modeling dust for optimization, long term analysis," in *Proc. Soiling Effect PV Modules Workshop*, Dubai, UAE, Apr. 7, 2016.

[4] L. L. Kazmerski *et al.*, "Fundamental studies of the adhesion of dust to PV module chemical and physical relationships at the microscale," in *Proc. IEEE 42nd Photovolt. Spec. Conf.*, 2015, pp. 1–7.

[5] M. Schweiger and W. Herrmann, "Electrical stability of PV modules in different climates," in *Proc. IEEE 43rd Photovolt. Spec. Conf.*, 2016, pp. 3685–3687.

[6] L. Simpson, M. Muller, M. Deceglie, D. Miller, and H. Moutinho, "The modeling of the effects of soiling, its mechanisms, and the corresponding Abrasion," Nat. Renew. Energy Lab., Golden, CO, USA, Tech. Rep. NREL/PR-5K00-66822, 2016.

[7] M. A. Bahattab *et al.*, "Anti-soiling surfaces for PV applications prepared by sol-gel processing: Comparison of laboratory testing and outdoor exposure," *Sol. Energy Mater. Sol. Cells*, vol. 157, pp. 422–428, 2016.

[8] R. K. Jones *et al.*, "Optimized cleaning cost and schedule based on observed soiling conditions for photovoltaic plants in central Saudi Arabia," *IEEE J. Photovolt.*, vol. 6, no. 3, pp. 730–738, May 2016.

[9] I. Nayshevsky, Q. Xu, G. Barahman, and A. Lyons, "Self-cleaning effects of the anti-soiling and anti-reflective textured fluoropolymer nano coatings," in *Proc. IEEE 44rd Photovolt. Spec. Conf.*, 2017, pp. 2285–2290.

[10] B. Mondal *et al.*, "Design and fabrication of a hybrid superhydrophobic–hydrophilic surface that exhibits stable dropwise condensation," *ACS Appl. Mater. Interfaces*, vol. 7, no. 42, pp. 23575–23588, 2015.

[11] K. K. Varanasi, M. Hsu, N. Bhate, W. S. Yang, and T. Deng, "Spatial control in the heterogeneous nucleation of water," *Appl. Phys. Lett.*, vol. 95, 2009, Art. no. 09410.

[12] L. Skinner and J. Sambles, "The Kelvin equation—A review," *J. Aerosol Sci.*, vol. 3, no. 3, pp. 199–210, 1972.

[13] H. B. Eral, D. J. C. M.'t Mannetje, and J. M. Oh, "Contact angle hysteresis: A review of fundamentals and applications," *Colloid Polym. Sci.*, vol. 291, no. 2, pp. 247–260, Feb. 2013.

[14] C. W. Extrand and A. N. J. Gent, "Retention of liquid drops by solid surfaces," *J. Colloid Interface Sci.*, vol. 138, pp. 431–442, 1990.

[15] A. M. Lyons and Q. F. Xu, "Center-side method of producing superhydrophobic surface," U.S. Patent 9 987 818, Jun. 5, 2018.

Authors' photographs and biographies not available at the time of publication.